An Algorithm for Mapping Precursory Topographic Features of Deep-seated Landslide A Case Study in Damaged Area in Typhoon Talas

Atsuko NONOMURA[1] and Shuichi HASEGAWA[1]

[1] Dept. of Safety Systems Construction Engineering, Kagawa University (Hayashicho 2217-20, Takamatsu 7610396, Japan)

*Corresponding author. E-mail: nonomura@eng.kagawa-u.ac.jp

In the deep-seated gravitationally deformed slopes, deep-seated landslides tend to be triggered by intensive rainfall. In order to mitigate the damages as much as possible, the distribution of deep-seated gravitational slope deformation is primary information for predicting and mitigating landslide damage beforehand. This study proposes and tests a simple algorithm for extracting deep-seated gravitationally deformed slope by analyzing 10-m resolution Digital Elevation Model (DEM) with windows of three sizes. Local relief is extracted with a large size window (2000 m by 2000 m) and middle size window (500 m by 500 m), and microtopography is extracted with a small size window (30 m by 30 m). The algorithm was derived and tested in Kii mountains, where deep-seated landslides were triggered by large amount of rainfall due to 2011 Typhoon Talas. The algorithm is useful for broadly extracting deep-seated gravitationally deformed slopes as deep-seated landslide susceptible slopes.

Key words: deep-seated landslide, DEM, gravitationally deformation

1. INTRODUCTION

Large and catastrophic deep-seated landslides have been triggered by earthquake or heavy rainfall in mountainous areas. The huge amount of debris often causes the secondary damage of a disaster, such as dammed river and outburst flooding, paralyzing road network, isolating a village (Chigira et al. 2003; Shou and Wang 2003; Wang et al. 2003; Chigira and Yagi 2006; Sato et al. 2007; Yagi et al. 2009; Chigira et al. 2010). Although the frequency of deep-seated landslides was very low, even a single event can destroy villages and damage hundreds of people. In order to mitigate the damage as much as possible, estimating the hazard and planning risk management should be one of the effective approaches.

Some deep-seated catastrophic landslides are known to have been preceded by deep-seated gravitational slope deformation that was expressed in the topography (Chigira and Kiho 1994; Chigira, 2009; Chigira et al., 2013).

Generally, the deep-seated gravitational deformed slopes have been recognized by interpreting linear depressions or scarps over upland gentle slopes on aerial photograph (Tabor 1971; Chigira 1992; Chigira and Kiho 1994, Geertsema et al. 2006b; Chigira et al. 2010). The results may vary among different mappers depending on their knowledge and experience. With recent developments in survey and computing technology, several geomorphological features have been investigated by using digital elevation models (DEMs). Many studies have proposed automatic or semi-automatic method for extracting susceptible slopes of landslide. Surface roughness is commonly used for estimating the degree of activity within a given slope; the more active the mass movement, the higher its surface roughness of each grid (McKean and Roering 2004; Glenn et al. 2006; García-Rodríguez et al. 2008; Kasai et al. 2009). Most grid-based approaches estimate landslide susceptibility without considering the surrounding major landforms (Dai and Lee 2002; Remondo et al. 2003; Santacana et al. 2003; Duman et al. 2006; Lee 2007; Hasegawa et al. 2009). As each grid is only a small part of larger topography, grid-based analysis is not always applicable to investigate susceptibility of deep-seated landslides.

The precursor topography of deep-seated landslide can be visually indicated using high resolution laser altimetry data with 5m or smaller ground resolution (Chigira et al. 2013). However, since the coverage of laser altimetry data is limited due to survey cost and the manual interpretation takes a lot of effort, it is necessary to develop any cheap and simple method for identifying the precursor topography of deep-seated landslide. For

widely identifying the deformed slopes as precursory topography of deep-seated landslide, it is necessary to develop methods for quickly identifying the topography of slope deformation using readily available data. In this study, 10-m resolution DEM (10-m DEM) was used as the input data. The data is processed by interpolating contour lines, which are delineated on 1:25,000 topographic maps based on aerial stereo photographs (Ardiansyah and Yokoyama 2002).

In Nonomura and Hasegawa (2013), a simple algorithm was proposed for extracting surface morphology of flexural toppled slopes (**Fig. 1(a)**) as one type of deep-seated gravitationally deformed slopes using a 10-m DEM. By using two windows, a small window (30 m by 30 m) and a large window (2000 m by 2000 m), surface morphology of flexural toppled slopes are extracted. This algorithm is useful for extracting flexural toppling on a steeply dipping slope, but it is not applicable to sliding on a dip slope because the topographic characteristics are different from each other. For extracting flexural toppled zones, we focused on upland gentle slopes surrounded by steep slopes, which are result of forward rotation of steeply dipping the strata by receiving load from overturned strata above them. On the other hand, sliding is a downslide movement of a soil mass and rock mass on the sliding surface occurring dominantly on a dip slope (**Fig. 1(b)** and **Fig. 1(c)**). Gravitationally deformed slopes with high susceptibility to sliding have gentle upland slopes with scarps, which are different from flexural toppling and not surrounded by steep slopes. The objective of this study is to develop a simple method for identifying gravitationally deformed slopes susceptible to sliding on a GIS platform.

2. TOPOGRAPHIC CHARACTERISTICS OF DEEP-SEATED GRAVITATIONAL DEFORMATION

The deep-seated gravitational deformation is precursor topography of deep-seated landslides. Deep-seated landslides are mostly categorized into flexural toppling and sliding. Flexural toppling occurs when individual steeply dipping strata bend forward under their own weight and transferred load from overlaying beds, and the flexural slip causes rotational movement (Adhikary et al., 1997)(**Fig. 1(a)**). As a result, flexural toppling produces uphill-facing scarps and multiple depressions on the gentle upland slopes. Failure at toppled slopes appears to be steep slopes. Since failures occur until all of the toppled rock mass is eroded away, steep

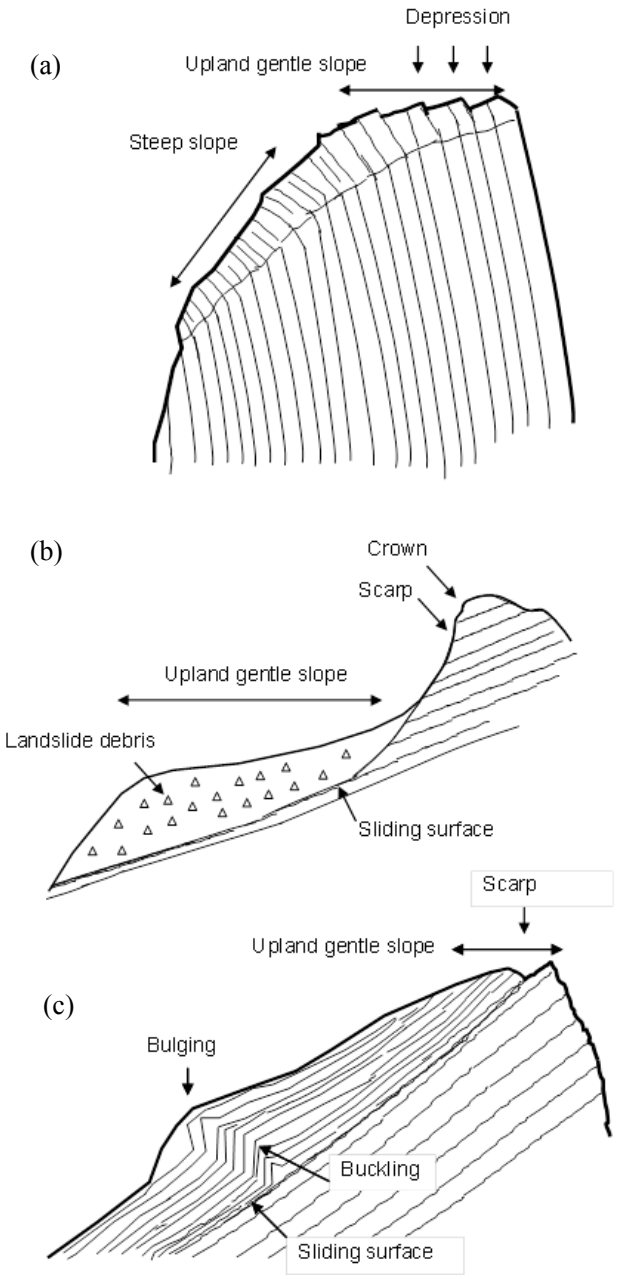

Fig. 1 Deep-seated gravitationally deformed structures (a) Flexural toppling (b) Sliding at old landslide (c) Sliding without old landslide

slopes are situated near the gentle upland slopes. For extracting flexural toppled zones, gentle grids (slope < 15°) surrounded by steep grids (slope > 50°) with multiple depressions were extracted.

On the other hand, sliding occur on a sliding surface or on relatively thin zones of intense shear strain, mainly on dip slopes. In many cases, old landslides were reactivated by intensive rainfall. Therefore, interpreting old landslide on aerial photography is one of the methods for identifying

susceptible slopes to sliding (Geertsema et al. 2006a). In 2011 typhoon Talas, many landslides occurred due to reactivation by intensive rainfall (Doshida 2012; Chigira et al. 2013). However, in some places, deep-seated landsides occurred, where old landslide was not identified on the pre-landslide topography. At these slopes, gravitational deformation was identified (Chigira et al. 2013). The movement of gravitational deformation does not occur simultaneously over the whole of what eventually becomes the sliding surface. Often the first signs of ground movements are cracks in the original ground surface along which the main scarp of the slide will form. The sliding surface is parallel to the slope. The deformed mass may gradually move downward, and the upper surface of the deformed mass tilts backward **(Fig. 1(c)**). As a result, lower part of the deformation may be formed by bulging of slopes, and as a result, depressions and scarps may be formed on the gentle upland slopes. In this study, an algorithm was proposed for extracting gravitationally deformed slopes susceptible to sliding; gentle upland slopes with scarps

3. STUDY AREA

The study area is Kii mountains located between 34°05'N and 33°30'N latitude and between 135°30'E and 135°52'E longitude in Kii Peninsula, Japan (**Fig. 2**). In the Kii Mountains, which are 100 km width and 100 km length, the elevation is over 1000 m at the center, and the maximum elevation reaches to 1915 m. The area is predominantly underlain by the Cretaceous to Paleogene-lower Miocene Shimanto accretionary complex. The complex consists of foliated mudstone, sandstone, acid tuff, chart, and greenstones (Hashimoto and Kimura, 1999)

In September 2011, catastrophic deep-seated landslides in this area were triggered by record breaking rainfall due to Typhoon Talas. The total rainfall recorded by the Kazeya rain gauge, which is the nearest weather station to the study area, reached 1,359 mm from 31st August to 4th September. It corresponds to two-thirds of the mean annual precipitation. The intensive rainfall induced many deep-seated landslides in this area. Most of the landslides are categorized into sliding (Chigira et al. 2013).

4. ALGORITHM

In this study, for detecting deep-seated landslide susceptible slopes, a simple algorithm is developed by modeling the surface morphology of deep-seated gravitational deformation as precursor topography of deep-seated landslides; linear depressions or scarps on gentle upland slopes. Gentle slopes are extracted by using slope angles with middle size window (500 m by 500 m). Upland slopes are extracted by using elevation difference within the large size window (2000 m by 2000 m). Depressions and scarps are extracted by using profile curvature (Mitášová and Hofierka 1993; Shary et al. 2002) with small size window (30 m by 30 m). Rules for extracting upland slopes and

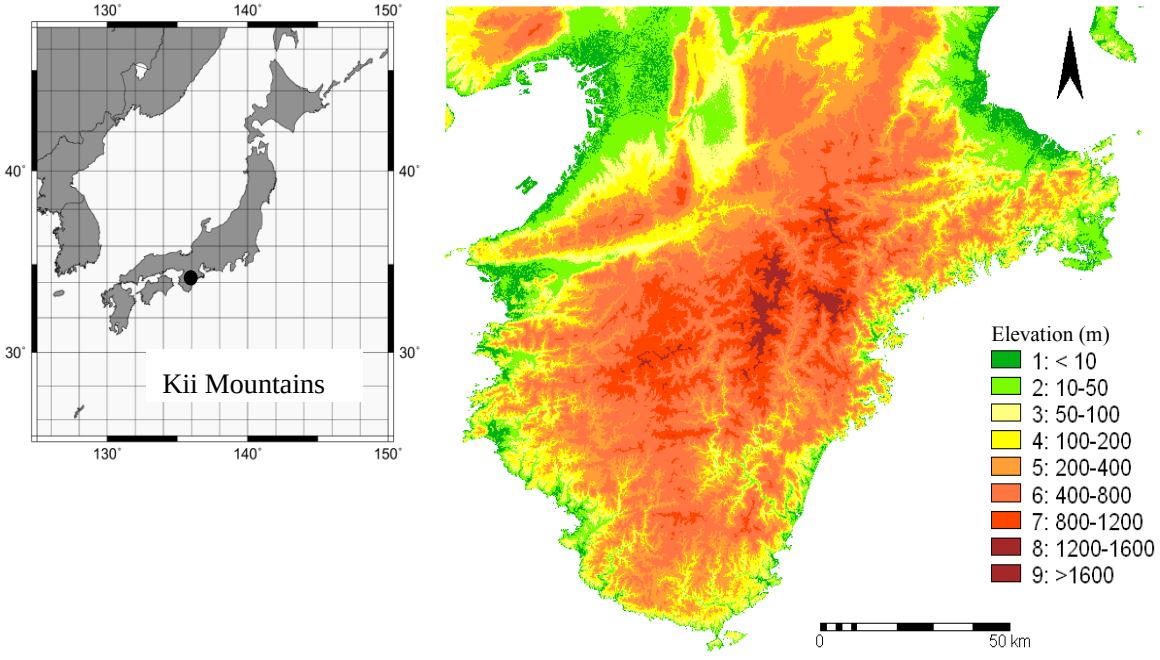

Fig. 2 Study area

depressions and scarps are the same as the rules for flexural toppling (Nonomura and Hasegawa, 2013). The algorithm is tested by applying on pre-landslide10-m DEM data in damaged areas by 2011 Typhoon Talas.

The algorithm was coded in Ruby, which is the object-oriented programming language, and applied to the DEM data.

4.1. DEM

As the input data, this study used a 10-m DEM produced by interpolating contour lines, which were delineated on 1:25,000 topographic map. The topographic map was drawn on aerial stereophotographs. DEM data of this type can be processed more easily and at lower cost than laser altimetry data.

The grid size of a DEM is one of the key parameters of the geomorphological analysis. In our proposed algorithm, slope and profile curvature were used as geomorphological parameters. For calculating slope, the higher the resolution, the more accurate the result is. For calculating curvatures to quantify concavity and convexity, a 1- to 3-m grid size is too small, and grids larger than 10 m are too coarse (Nonomura et al. 2009). For calculating curvatures to identify concavity and convexity, the most appropriate grid size is 5-6 m, although 10-m DEM data are still usable (Nonomura et al. 2009). On the other hand, a large grid size is adequate for reducing small-scale topographic variation and analyzing regional characteristics (Hengl 2006). Nonomura and Hasegawa (2013) showed that the 10-m DEM is usable in automatically extracting surface morphology of flexural toppled slopes in a regional scale.

4.2. Gentle upland slope extraction

Two rules of the algorithm are developed to extract

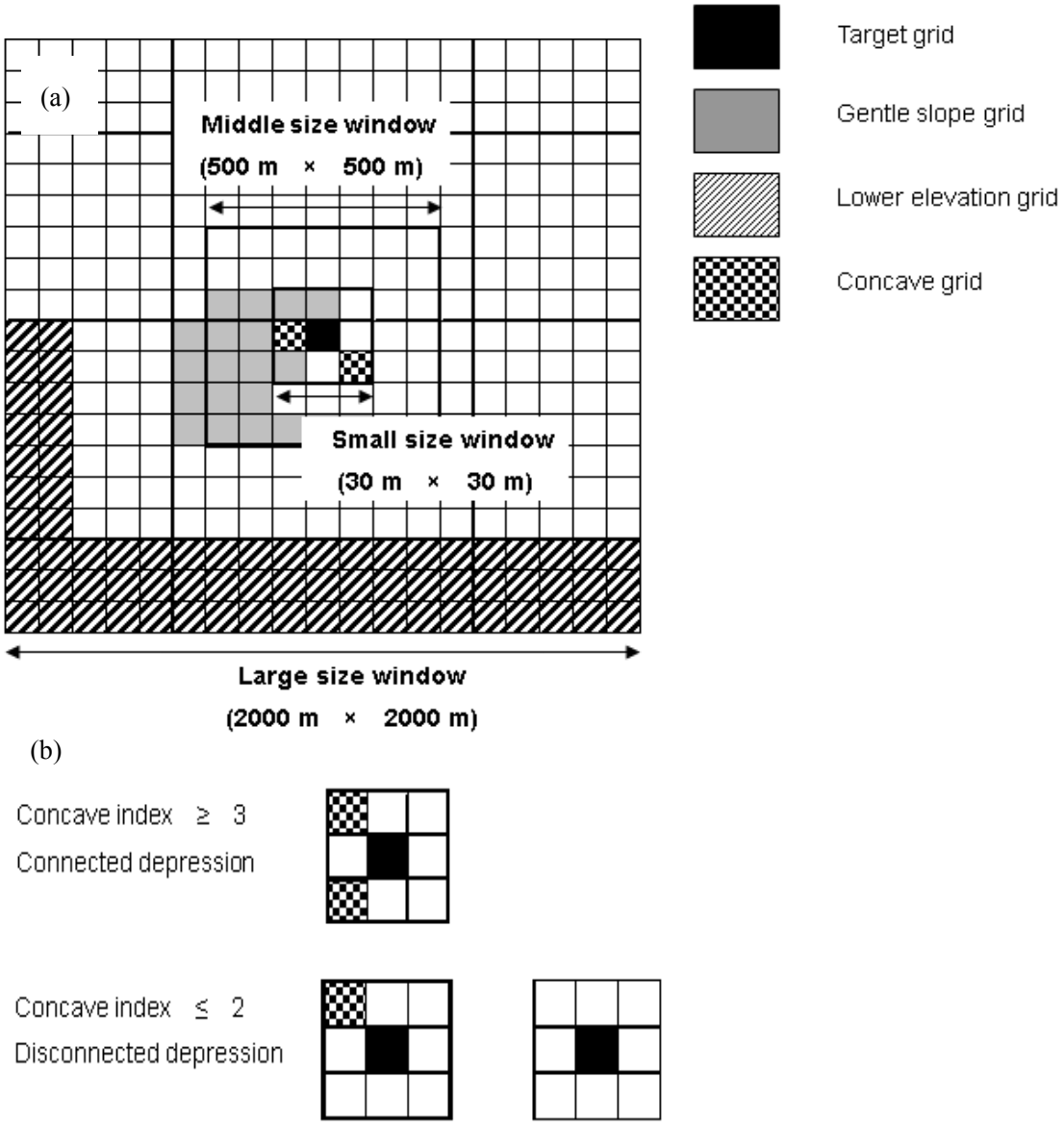

Fig. 3 Diagram of the algorithm (a) large and middle size window (b) small size window

gentle upland slopes, which have been formed by deep-seated gravitational deformation. Rule1 extracts gentle slopes and Rule 2 extracts upland slopes (**Fig. 3(a)**). In this study, the criterion for adjacency is applied by defining the window size.

Rule 1 extracts gentle slopes. If the slope of the focal grid is gentle and it is surrounded by grids of gentle slope, the focal grid is regarded to be a part of a gentle slope. In this study, the middle size window was defined to be 500 m x 500 m square to specify surrounding grids of the target grid. If the slope of the focal grid is smaller than 30° (slope < 30°) and more than 20 % of grids show slope < 30° within the surrounding grids extracted with middle size window, the focal grid is regarded to be a part of gentle slopes.

Rule 2 extracts upland slopes. If the elevation of the focal grid is higher than that of adjacent grids, the grid is regarded to be a part of upland slope. The criterion for elevation difference is defined to be 200m and the adjacently located grids were extracted with large size window. In this study, the large size window was defined to be 2000m x 2000m square to compare the elevation of the target grid with adjacently located grids. If more than 5% of grids are 200 m lower than the focal grid within the large size window (2000m x 2000m), the focal grid is regarded to be a part of an upland slope. Rule 2 is the same as upland slopes extraction of flexural toppling (Nonomura and Hasegawa 2013).

It is assumed that by satisfying Rule 1 and Rule 2, the focal grid is a part of a gentle upland slope.

4.3. Extraction of linear depressions and scarps

Since linear depressions and scarps are concave along the slopes, the direction and degree of the curvature are quantified by calculating profile curvatures (Mitášová and Hofierka 1993; Shary et al. 2002). The concave grid is regarded as a part of depression or a scarp, and a series of connected concave grids is regarded as a linear depression or a scarp (**Fig. 3(b)**). In this study the thresholds of concavity is defined to be curvature > 0.01/m), and the continuity is approximated by counting the number of concave grids adjacent to the focal concave grid in a 3 by 3 grids window, which was called "small size window" in this study.

The number of concave grids within the small window (including the focal grid) is defined to be the concave index. If the focal grid is concave and concave index ≥ 3, it means that the focal grid connects to two or more concave grids within the small window and the focal grid is a part of a linear depression or a scarp. If the focal grids is concave and concave index =2, the focal grid is not assigned to be a part of a linear depression or a scarp, because the focal concave grid connects to only one concave grid within the small window. The focal grid is concave and the concave index =1 means that only the focal grid is concave within the small window. The concave index =0 means that the focal grid is not concave. Rule 3 is the same algorithm as for extracting multiple depression of flexural toppling (Nonomura and Hasegawa 2013).

Rule3: If the focal grid is concave and the concave index ≥ 3, the focal grid is regarded as a part of a linear depression or a scarp.

4.4. Extraction of precursor topography of deep-seated landslide susceptible slopes

Gentle upland slopes are extracted by applying Rule 1 and Rule 2. Linear depressions and scarps are extracted by applying Rule 3. By overlaying the linear depressions and scarps on the gentle upland slopes, deep-seated gravitational deformations are extracted as precursor topography of deep-seated landslide.

5. RESULTS

To test the algorithm, the extracted morphology is compared with visualized airborne laser altimetry pre-landslide 5-m DEM, field observation and published survey record about the deep-seated landslides triggered by large amount of rainfall due to 2011 Typhoon Talas.

For testing the algorithm, a test area was selected surrounding of Akatani-east landslides scars, which is delineated using visualized laser altimetry DEM data with red relief image map method, which was developed by Asia Air Survey (Japan Patent No 3670274/4272146). The source area and the volume of the landslide is reported 191,200 m^2 and 2.1×10^6 m^3 (Chigira et al. 2013).

Fig. 4 compared the extracted topography by the algorithm with visualized laser altimetry data around Akatani-east landslide. Both data are processed by using pre-landslide data. Fig. 4(a) shows the extracted upland gentle slopes (yellow) with linear depressions and scarps (blue) by using pre-landslide DEM. Chigira et al (2013) reported that upland gentle slope with scarps and depressions were interpreted on the visualized laser altimetry pre-landslide DEM. In order to validate the algorithm, the extracted topographies (Fig. 4(a)) were compared with visualized laser altimetry 5-m DEM data (Fig.4(b)) . Fig.4(b) is visualized high resolution laser altimetry data by Red Relief Image Map (RRIM), which is stereoscopic visualization

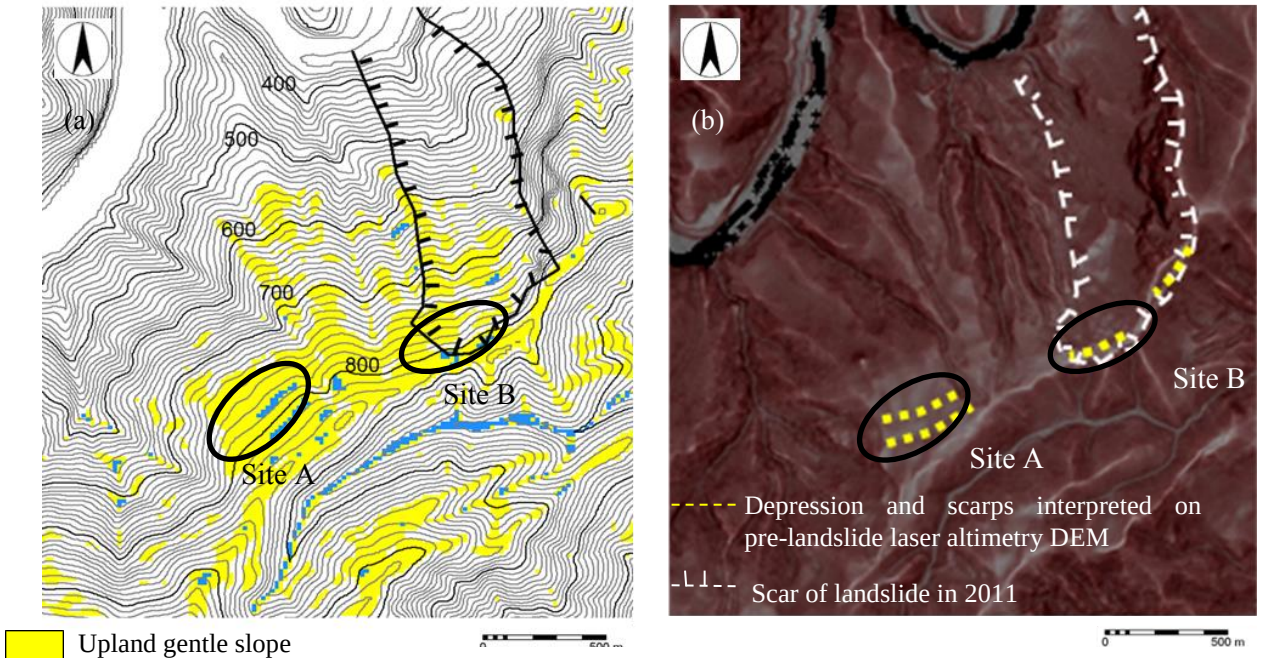

Fig.4 Pre-cursor topography of deep-seated landslide (a) The result of the proposed algorithm. (b) Visualized laser altimetry DEM with interpreted depression and scarps.

method developed by Asia Air survey (Japan Patent No 3670274/ 4272146). Interpreted depressions and scarps are delineated on the RRIM with yellow dot lines.

Over upland gentle slopes (yellow grids), extracted connected concave grids (blue grids) correspond to some part of the interpreted scarps on the laser altimetry DEM near crown of the landslides in 2011 (site B). All of depressions and scarps over upland gentle slopes cannot be extracted. It is probably because the original data and their accuracy are different and pixel size is also different.

Neighborhood area of the Akatani-east landslide (at site A), deep-seated gravitational deformed slopes were extracted; scarps on gentle upland slopes. It was identified on the visualized laser altimetry DEM and in our field survey. In 2011, no landslide occurred in the site B. According to topographical characteristics, this slope might be loosened. So, deep-seated landslide might occur at this slope in future.

6. CONCLUSION

Our method can be used to extract precursor topography of deep-seated landslides, which will slide down from the ridge top without old landslide. Upland gentle slopes with linear depressions are focused as topographic characteristics of loosened slopes. Because of data accuracy, all of the precursor topographies cannot be extracted, but some part of them is easily indicated. The proposed algorithm can be used simple screening method for extracting gravitationally deformed slopes as deep-seated landslide susceptible slopes.

The algorithm cannot be applied to extract precursor topography in slopes that are susceptible to the reactivation of old landslides. The interpreted old landslide topography and result of our algorithm can compensate each other for estimating deep-seated landslide susceptible slopes.

Acknowledgements

This work was supported by JSPS Grant-in-Aid for Young Scientists (B)(No. 25750152). The laser altimetry data was provided by the Ministry of Land, Infrastructure, Transportation and Tourism, Japan.

REFERENCES

Ardiansyah, P.O.D. and Yokoyama, R. (2002): DEM generation method from contour lines based on the steepest slope segment chain and a monotone interpolation function. ISPRS Journal of Photogrammetry and Remote Sensing, Vol. 57, pp.86-101.

Chigira, M. (1992): Long-term gravitational deformation of rocks by mass rock creep. Engineering Geology, Vol. 32, pp.157-184.

Chigira, M. (2009): September 2005 rain-induced catastrophic rockslides on slopes affected by deep-seated gravitational deformations, Kyushu, southern Japan. Engineering Geology, Vol. 108, pp. 1-15.

Chigira, M. and Kiho, K. (1994): Deep-seated rockslide-avalanches preceded by mass rock creep of

sedimentary rocks in the Akaishi Mountains, central Japan. Engineering Geology,Vol. 38, pp. 221-230.

Chigira, M., Tsou, C., Matsushi, Y., Hiraishi, N. and Matsuzawa, M. (2013): Topographic precursors and geological structures of deep-seated catastrophic landslides caused by Typhoon Talas, Geomorphology, Vol. 201, pp.479-493.

Chigira, M., Wang, W.N., Furuya, T. and Kamai, T. (2003): Geological causes and geomorphological precursors of the Tsaoling landslide triggered by the 1999 Chi-Chi earthquake, Taiwan. Engineering Geology, 68, pp.259-273.

Chigira, M., Wu, X., Inokuchi, T. and Wang, G., (2010): Landslides induced by the 2008 Wenchuan earthquake, Shichuan, China. Geomorphology, Vol. 118, pp. 225-238.

Chigira, M., and Yagi, H. (2006): Geological and geomorphological characteristics of landslides triggered by the 2004 Mid Niigta prefecture earthquake in Japan. Engineering Geology, 82, pp. 202-221.

Dai, F.C. and Lee, C.F. (2002): Landslide characteristics and slope instability modeling using GIS, Lantau Island, Hong Kong. Geomorphology, Vol. 42, pp. 213-228.

Doshida, S. (2012): Feasibility of use of landslide maps for assessing catastrophic landslides. Journal of the Japan Society of Erosion Control Engineering, Vol. 65, pp. 52-55.

Duman, T.Y., Can, T., Gokceoglu, C., Nefeslioglu, H.A. and Sonmez, H. (2006): Application of logistic regression for landslide susceptibility zoning of Cekmece Area, Istanbul, Turkey. Environmental Geology, Vol. 51, pp. 241-256.

García-Rodríguez, M.J., Malpica, J.A., Benito, B. and Díaz, M. (2008): Susceptibility assessment of earthquake-triggered landslides in El Salvador using logistic regression. Geomorphology, Vol. 95, pp. 172-191.

Geertsema, M., Clague, J.J., Schwab, J.W., Evans, S.G. (2006a) An overview of recent large catastrophic landslides in northern British Columbia, Canada. Engineering Geology, Vol. 83, 120-143

Geertsema, M., Hunger, O., Schwab, J.W. and Evans, S.G. (2006b) A large rockslide-debris avalanche in cohesive soil at Pink Mountain, northeastern British Columbia, Canada. Engineering Geology, Vol. 83, 64-75.

Glenn, N.F., Streutker, D.R., Chadwick, D.J., Thackray, G.D. and Dorsch, S.J. (2006): Analysis of LiDAR-derived topographic information for characterizing and differentiating landslide morphology and activity. Geomorphology, Vol. 73, pp.131-148.

Hasegawa, S., Dahal, R.K., Nishimura, T., Nonomura, A. and Yamanaka, M. (2009): DEM-based analysis of earthquake-induced shallow landslide susceptibility. Geotechnical and Geological Engineering, Vol. 27, 419-430.

Hashimoto, Y. and Kimura, G.: (1999): Underplating process from melange formation to duplexing: example from the Cretaceous Shimanto Belt, Kii Peninsula, southwest Japan, Vol. 18, pp. 92-107.

Hengl, T. (2006): Finding the right pixel size. Computers & geosciences, Vol. 32, pp. 1283-1298.

Kasai, M., Ikeda, M., Asahina, T. and Fujisawa, K. (2009): LiDAR-derived DEM evaluation of deep-seated landslides in a steep and rocky region of Japan. Geomorphology, Vol. 113, pp. 57-69.

Lee, S. (2007): Application and verification of fuzzy algebraic operators to landslide susceptibility mapping. Environmental Geology, Vol. 52, pp. 615-623.

McKean, J. and Roering, J. (2004): Objective landslide detection and surface morphology mapping using high-resolution airborne laser altimetry. Geomorphology, Vol. 57. pp. 331-351.

Mitášová, H. and Hofierka, J. (1993): Interpolation by regularized spline with tension: 2. Application to terrain modeling and surface geometry analysis. Mathematical Geology, Vol. 25, pp. 657-669.

Nonomura, A. and Hasegawa, S. (2013): Regional extraction of flexural-toppled slopes in epicentral regions of subduction earthquakes along the Nankai Trough using DEMs. Environ Earth Sci Vol. 68. pp. 139-149.

Nonomura, A., Hasegawa, S., Tomida, U., Mori, H. and Yatabe, R. (2009): Seismic hazard evaluation method along highway using digital elevation model. Symposium of slope collapse mechanism stability evaluation for rainfall and earthquake, pp. 369-374 (in Japanese)

Remondo, J., González, A., Terán, J.R.D., Cendrero, A., Fabbri, A. and Chung, C.F. (2003): Validation of landslide susceptibility maps; examples and applications from a case study in Northern Spain. Natural Hazards, 30. pp. 437-449.

Santacana, N., Baeza, B., Corominas, J., Paz, A.D., and Marturiá, J. (2003): A GIS-based multivariate statistical analysis for shallow landslide susceptibility mapping in La Pobla de Lillet Area (Eastern Pyrenees, Spain). Natural Hazards, Vol. 30. pp. 281-295.

Sato, H.P., Hasegawa, H., Fujiwara, S., Tobita, M., Koarai, M., Une, H. and Iwahashi, J. (2007): Interpretation of landslide distribution triggered by the 2005 Northern Pakistan earthquake using SPOT 5 imagery. Landslides, Vol. 4. pp. 113-122.

Shary, P.A., Sharaya, L.S. and Mitusov, A.V. (2002) Fundamental quantitative methods of land surface analysis. Geoderma, Vol. 107, pp. 1-32.

Shou, K.J. and Wang, C.F. (2003) Analysis of the Chiufengershan landslide triggered by the 1999 Chi-Chi earthquake in Taiwan. Engineering Geology, 68: 237-250.

Tabor, R.W. (1971) Origin of ridge-top depressions by large-scale creep in the Olympic Mountains, Washington. Geological Society of America Bulletin 82: 1811-1822.

Wang, W.N., Chigira, M. and Furuya, T. (2003): Geological and geomorphological precursors of the Chiu-fen-erh-shan landslide triggered by the Chi-chi earthquake in central Taiwan. Engineering Geology, Vol. 69. pp. 1-13.

Yagi, H., Sato, G., Higaki, D., Yamamoto, M. and Yamasaki, T., (2009): Distribution and characteristics of landslides induced by the Iwate-Miyagi Nairiku Earthquake in 2008 in Tohoku District, Northern, Japan. Landslides, Vol. 6. pp. 335-344.

Ashida, K. and Takahashi, T. (1980): Study on debris flow control-hydraulic function of grid type open dam, Annuals. Disaster Prevention Res. Inst., Kyoto Univ., Vol. 23B-2, pp. 1-9 (in Japanese with English abstract)